JOURNAL OF SOLID STATE CHEMISTRY **123,** 73–82 (1996)
ARTICLE NO. 0154

Convergent Beam Electron Diffraction and High Resolution Electron Microscopy of $CaFeTi_2O_6$ Perovskite

Nan Yao,* Alexandra Navrotsky,*,† and Kurt Leinenweber‡

*Princeton Materials Institute, Princeton University, Princeton, New Jersey 08540; †Department of Geological and Geophysical Sciences, Princeton University, Princeton, New Jersey 08540; ‡Department of Chemistry, Arizona State University, Tempe, Arizona 85287

Received June 29, 1995; in revised form October 12, 1995; accepted January 23, 1996

A new calcium iron(II) titanate ordered perovskite, $CaFeTi_2O_6$, synthesized at 12–15 GPa and 1200–1400°C has been studied using convergent beam electron diffraction (CBED) and high-resolution transmission electron microscopy (HREM) techniques. CBED and selected area diffraction (SAD) patterns confirm that $CaFeTi_2O_6$ is tetragonal with a = 7.51 ± 0.02 Å, c = 7.54 ± 0.02 Å. The tetragonal structure is consistent with the symmetry of $P4_2/nmc$ proposed on the basis of X-ray diffraction studies. A $CaFeTi_2O_6$ crystal was studied at both ambient temperature and 84 K. *In situ* experiments show no phase transformation upon cooling. High resolution imaging and nanobeam analysis reveal three types of morphology. In addition to the major nearly perfect perovskite phase, this material contains two sizes of iron precipitates. One size class averages 4 nm in diameter and the other 15 nm in diameter. Crystalline perovskite-like domains with a high degree of disorder were also observed. The formation of this type of domain may be related to local variations of stoichiometry with considerable oxidation. The coexistence of reduced and oxidized regions in the same specimen is noteworthy, and probably indicates incomplete equilibration during high pressure synthesis.

1. INTRODUCTION

A new calcium iron(II) titanate compound, $CaFeTi_2O_6$, was recently synthesized from an equimolar mixture of $CaTiO_3$ and $FeTiO_3$ at 12–15 GPa and 1200–1400°C (1, 2). This material is interesting both as a possible high pressure mineral in the Earth's mantle and as an example of a rather rare group of ordered perovskites, namely these with ordering of cations of like charge but different size on the A sites. X-ray diffraction studies show that $CaFeTi_2O_6$ has a variant of the perovskite structure and crystallizes in the tetragonal space group $P4_2/nmc$ with lattice parameter a = 7.5157(2) Å, c = 7.5548(2) Å (1). Although the X-ray diffraction technique forms the basis of accurate determination of lattice parameters and crystal symmetry, it provides structural information averaged over many unit cells and no information about structural variations on the nanoscale. Convergent beam electron diffraction (CBED) and high resolution electron microscopy (HREM) offer new possibilities for crystal structure analysis (3–5). CBED and HREM techniques are very attractive because they permit local rather than statistically averaged data for a large sample. CBED can study very small grains and precipitates in mixed-phase material and determine structure and symmetry of individual domains. When this information is supplemented by chemical data from energy dispersive X-ray (EDX) or parallel electron energy loss (PEELS) spectra, the phase in question often can be uniquely identified. In the present report, we discuss the structure and symmetry of $CaFeTi_2O_6$, based on a new study using CBED and HREM techniques.

2. EXPERIMENTAL

The sample had been synthesized at 12 GPa and 1400°C using the USSA2000 multivanvil press at the Center for High Pressure Research, Stony Brook, NY, as described previously (1, 2). The $CaFeTi_2O_6$ powder sample was ground in an agate mortar under purified methanol. A drop of the resulting suspension was placed on a copper grid coated with holey-carbon film. To avoid or at least minimize surface contamination, specimens were immediately transferred to the microscope air lock where they were dried out during the pump-down process. This procedure did not, however, always lead to a completely clean surface—a thin amorphous layer of perhaps 5–10 Å often still covered the crystal surface. CBED studies were performed on a Philips-CM20 ST transmission electron microscope operated at 120 keV under moderate vacuum conditions over the range 10^{-6}–10^{-7} Torr. A Gatan double tilt, liquid-nitrogen-cooled specimen holder was also used. The nanobeam analysis reported in this paper was carried on a JEM 2010F TEM operated at 200 KeV.

0022-4596/96 $18.00

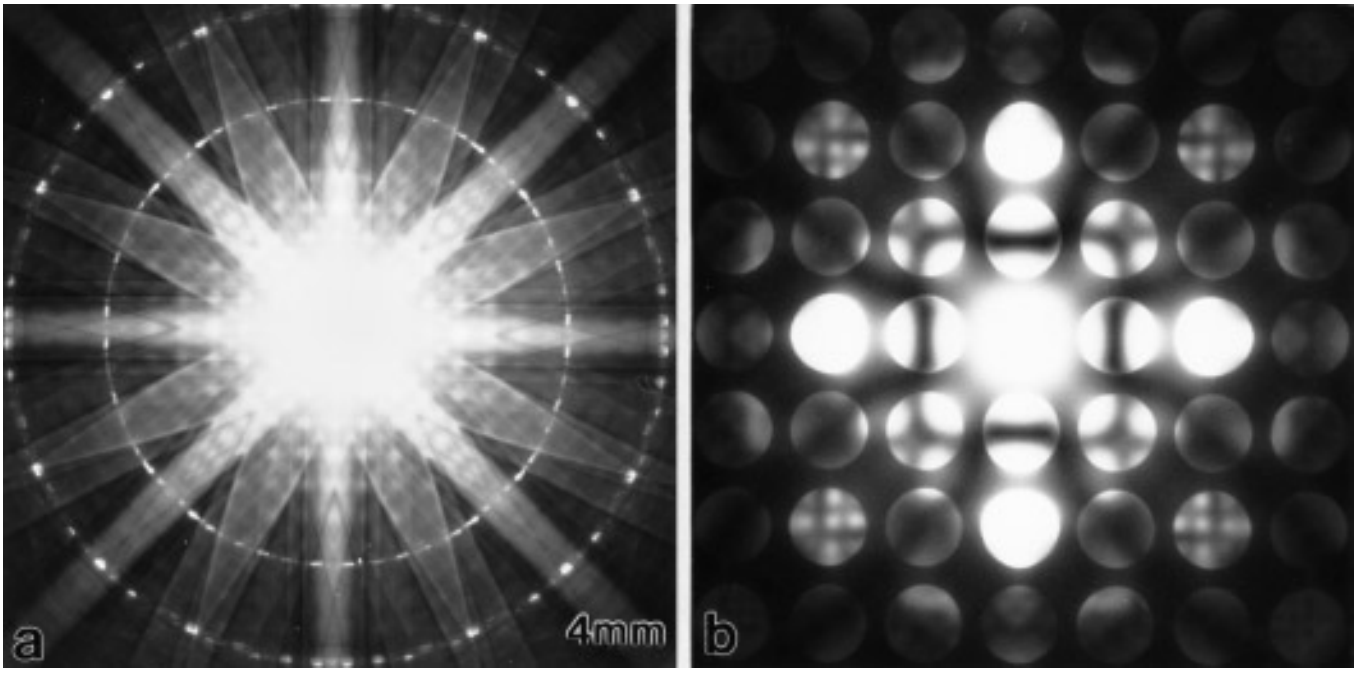

FIG. 1. Convergent beam electron diffraction pattern along [001] zone axis, with (a) a whole CBED pattern and (b) details from ZOLZ reflection in (a). Both (a) and (b) show a symmetry of 4*mm*.

This instrument represents a new generation of high-resolution analytical TEM (only recently commercially available). With the newly designed Schottky field emission gun, this instrument can provide an electron probe of less than 1 nm in size with ~500 pA in the beam current (the LaB_6 gun in a conventional TEM can only provide a beam current of 1 pA for the similar spot size). This unique capability makes this microscope an excellent tool to carry on the X-ray, EELS, and electron diffraction analysis at the subnanometer scale. The EDX analysis was performed

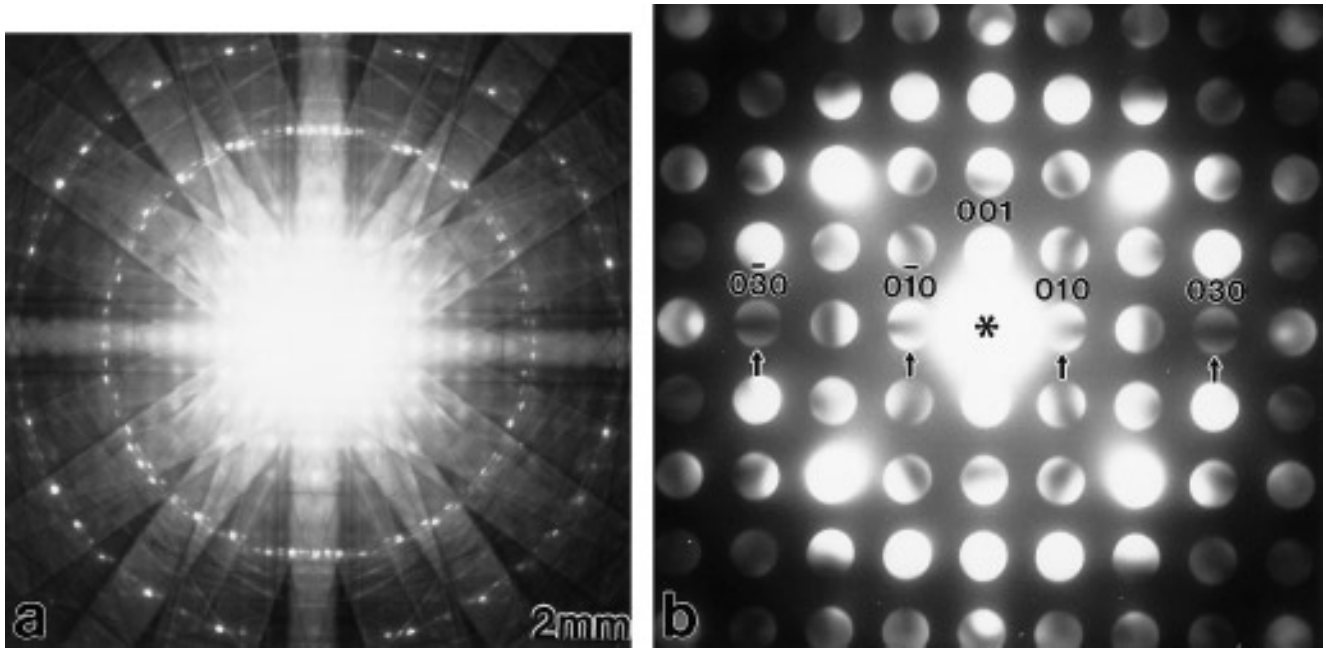

FIG. 2. Convergent beam electron diffraction pattern along [100] zone axis, with (a) a whole CBED pattern and (b) details from ZOLZ reflection in (a). Both (a) and (b) present a symmetry of 2*mm*.

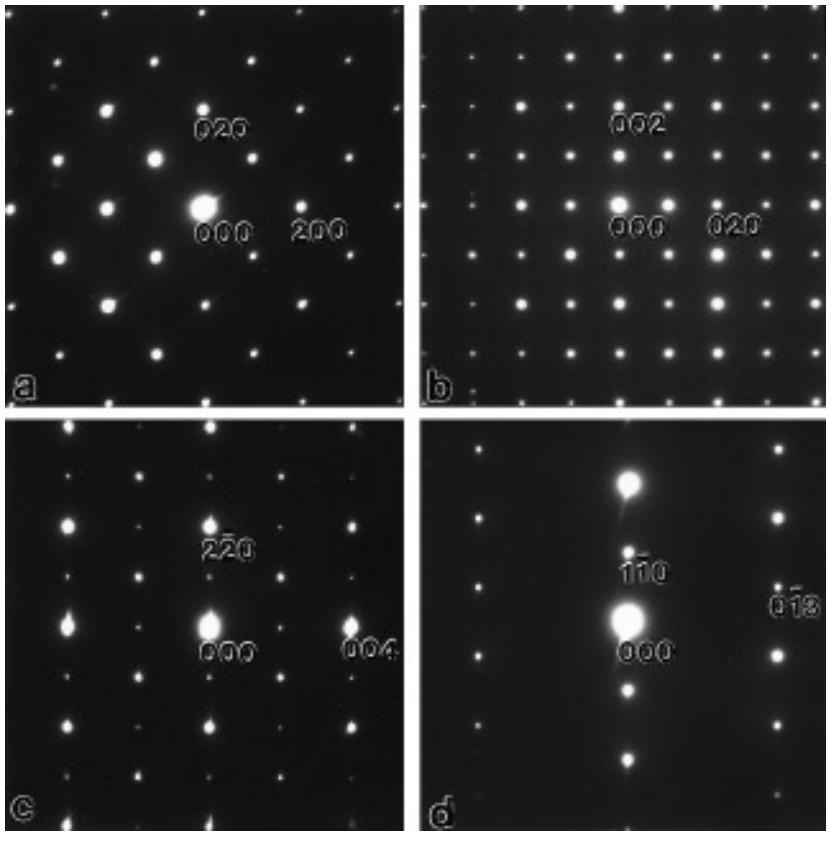

FIG. 3. Selected-area diffraction patterns obtained along high-symmetry zone axes, with (a) [001], (b) [100], (c) [110], and (d) [331]. Detailed measurements from these patterns show that $CaFeTi_2O_6$ is tetragonal with $a = 7.51 \pm 0.02$ Å, $c = 7.54 \pm 0.02$ Å.

using an ultrathin-window detector which can extend the range of element analysis to a lighter element, including O, N, C, and B ($Z = 5$). The spectra were obtained with a collecting time between 60 to 120 sec, and doubly checked for each crystal domain before processing. The elemental concentration was obtained by applying a standard quantification program in the Tracor Northern 5500-II multichannel analyzer to the X-ray spectra.

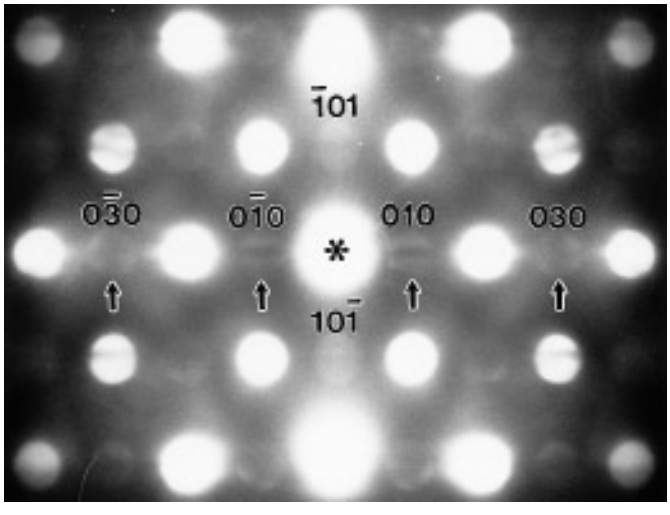

FIG. 4. Convergent beam electron diffraction pattern showing ZOLZ reflections along [101] zone axis at 120 KeV.

The $CaFeTi_2O_6$ crystal is tetragonal and the difference between lattice parameter a and c is less than 0.4%. The identification of crystal structure along two highest zone axes [100] and [001] is rather difficult by conventional selected-area electron diffraction. However, this can be accomplished by CBED. This facilitates the accurate determination of the full crystal symmetry and lattice parameters. The CBED patterns were acquired at both ambient and liquid nitrogen temperature. The contaminant films caused by the residual hydrocarbon vapor inside the microscope column can seriously distort the symmetries of the patterns and point disorder quickly ''smears-out'' the high angle scattering. Cooling the specimen from 300 to 84 K not only eliminates contamination but also reduces electron beam heating and radiation damage. However, caution needs to be taken when one examines crystals of unknown structure and symmetry at low temperature. Variations in specimen temperature could induce phase change, which might complicate the identification of the crystal structure in question (6). We have carefully compared CBED patterns obtained at both ambient and low

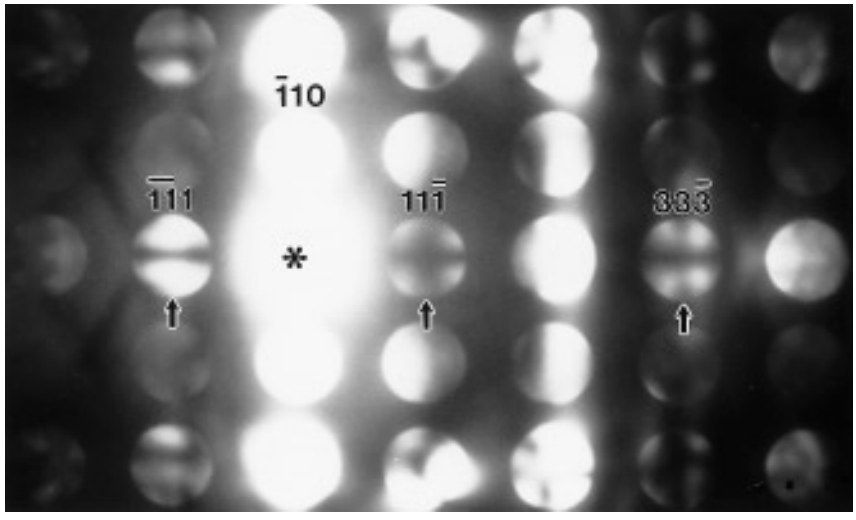

FIG. 5. Convergent beam electron diffraction pattern showing ZOLZ reflections along [112] zone axis at 120 KeV.

temperature for $CaFeTi_2O_6$ crystal, and no visible variations in crystal structure and symmetry were found.

3. RESULTS AND DISCUSSION

3.1. Lattice Parameter Determination

Convergent beam electron diffraction patterns at high-symmetry zone axis orientation provide both two- and three-dimensional information about crystal structure. The zero-order-Laue-zone (ZOLZ) is a two-dimensional section of the reciprocal lattice, thus it only provides information on lattice planes perpendicular to the zone axis. Information in the third dimension requires diffraction from the first-order-Laue-zone (FOLZ). The spacings between the adjacent reciprocal lattice layers in the direction of the incident electron beam, H, can be determined by measuring the radius (G) of the FOLZ ring, with $H = 0.5\,\lambda G^2$, where G (Å)$^{-1} = R/L$, R is the radius of the FOLZ ring in cm, L is the camera length in cmÅ, and λ (Å) is the wavelength of the electrons. Using a small electron probe size and large angular view (small camera length), one can uniquely determine the crystal structure of very small particles. The determination of $CaFeTi_2O_6$ lattice parameter was based mainly on the calculation from one zone axis CBED pattern collected from a single crystal. Figure 1a is a [001] low-camera-length CBED pattern obtained at 120 KeV. By measuring the radius of the FOLZ ring, the H^{-1} value was determined to be 7.54 ± 0.02 Å. The center part of Figure 1b is a ZOLZ pattern which consists of a square array of discs. The calculation of the sides of the square gives a lattice constant of 7.51 ± 0.02 Å, and these ZOLZ reflections were indexed as (100) and (010). Further calculations from other zone axes SAD patterns such as Figs. 3a–3d, and ZOLZ CBED patterns (Figs. 2b, 4, and 5) are in good agreement with the above measurement. Therefore, we have confirmed that $CaFeTi_2O_6$ is tetragonal with $a = 7.51 \pm 0.02$ Å, $c = 7.54 \pm 0.02$ Å.

TABLE 1
Four Space Groups Belonging to Point Group 4/*mmm* with Lattice Type (P)

Space group \ Incident beam direction	[100]		[*h*0*l*]		[*hhl*]	
129 $P4/nmm$	$0k0$	$A_2\ B_2$	$0k0$	$A_2\ B_2$		
$P4/n2_1/m2/m$	$n, 2_{12}$	$A_3\ B_3$	2_1	B_3		
	$0k0$	$A_2\ B_2$	$h0l_0$	$A_2\ B_2$		
130 $P4/ncc$	$n, 2_{12}$	$A_3\ B_3$	c_1	A_3	hhl_0	$A_2\ B_2$
$P4/n2_1/c2/c$	001		$0k0$	$A_2\ B_2$	c_2	A_3
	c_{12}	A_3	2_1	B_3		
137 $P4_2/nmc$	$0k0$	$A_2\ B_2$	$0k0$	$A_2\ B_2$	hhl_0	$A_2\ B_2$
$P4_2/n2_1/m2/c$	$n, 2_{12}$	$A_3\ B_3$	2_1	B_3	c	A_3
	$0k0$	$A_2\ B_2$	$h0l_0$	$A_2\ B_2$		
138 $P4_2/ncm$	$n, 2_{12}$	$A_3\ B_3$	c	A_3		
$P4_2/n2_1/c2/m$	001		$0k0$	$A_2\ B_2$		
	c_2	A_3	2_1	B_3		

3.2. Point Group Determination

There are several space groups within this crystal system that would be indistinguishable by electron diffraction limited to only selected-area diffraction or microdiffraction techniques. Fortunately, CBED makes it possible to examine the diffraction symmetry of key orientations of the crystal and therefore determine the point-group symmetry (3–10). This information, along with the dynamic extinc-

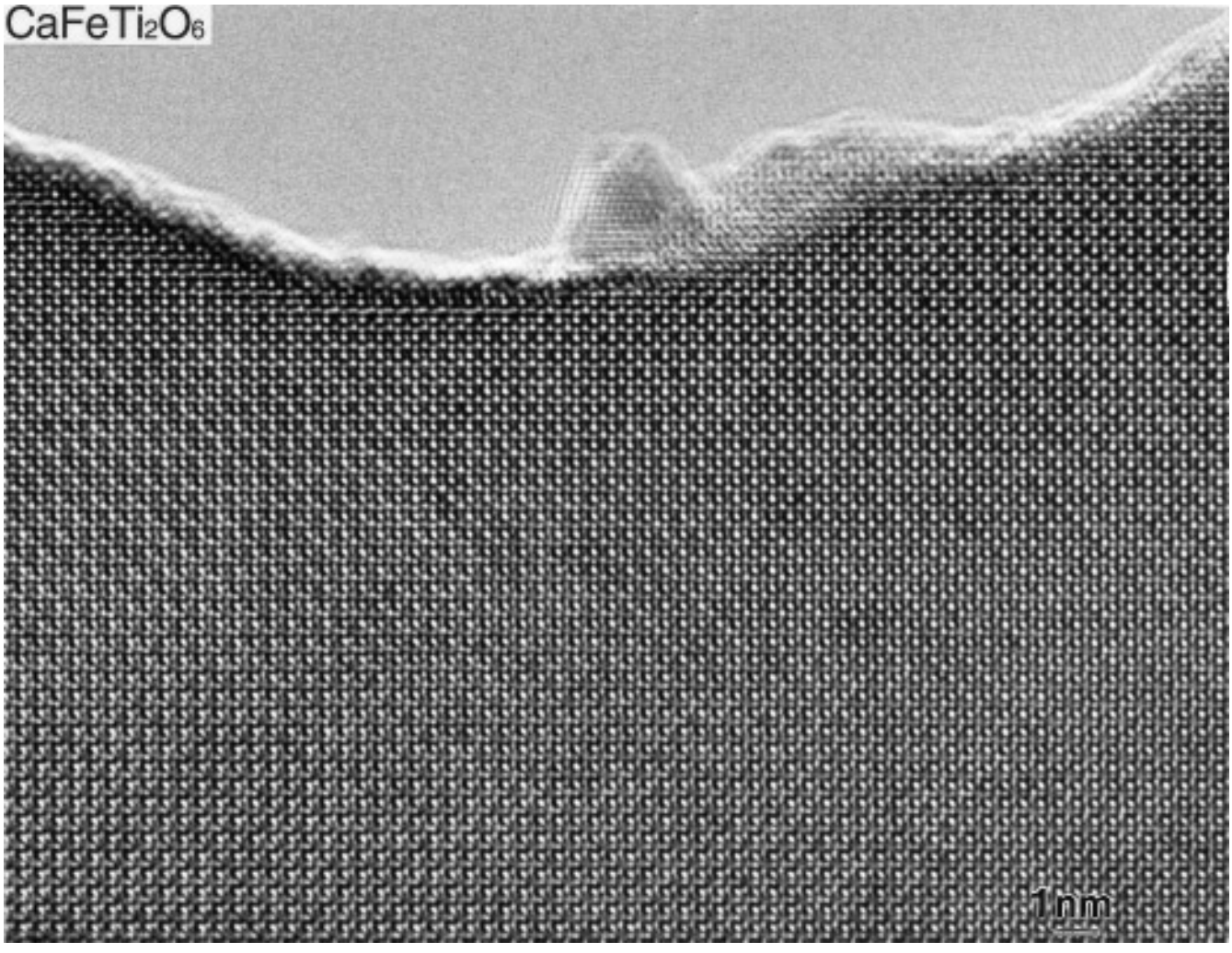

FIG. 6. High resolution lattice image of $CaFeTi_2O_6$ viewed along [001] zone axis at 200 KeV.

tion information on systematic absences, can be used to determine the crystallographic space group uniquely. Both two- and three-dimensional information of crystal symmetry elements can be obtained from CBED patterns at high-symmetry zone axis orientation taken with a wide angular view of the back focal plane of the objective lens. One such pattern is shown in Fig. 1, which is obtained with an electron probe size of 10 nm at 120 KeV. Figure 1a is a low-camera-length pattern at [001] on-zone-axis and Fig. 1b is a long-camera-length pattern showing the central portion of Fig. 1a. These patterns indicate the presence of a fourfold rotation axis along the *c* direction with four mirrors coincident with (100), (010), (110), and $(1\bar{1}0)$ lattice planes. Along with fine details in the pattern (Fig. 1a) of isotropic elastic–inelastic scattering or ''Kikuchi lines,'' this analysis suggests possible diffraction groups of 4*mm* or 4*mm*1*R*. Examination of the CBED pattern symmetry tables (5) reveals that a whole pattern symmetry of 4*mm* can arise from point group 4*mm*, and 4*mm*1*R* can arise from point group 4/*mmm* or *m*3*m*. According to previous electron diffraction studies of the lattice parameter, the tetragonal unit cell of $CaFeTi_2O_6$ is not compatible with cubic symmetry and the choice of point group *m*3*m* can be eliminated. To further distinguish two remaining possible point groups, it is necessary to find out whether the third mirror plane perpendicular to the *c* axis exists. Figure 2 shows a [100] zone axis CBED pattern collected under the same experimental conditions. Both HOLZ (Fig. 2a) and ZOLZ (Fig. 2b) reflections of this pattern show a symmetry of 2*mm*, with (010) and (001) mirror planes, giving a two-fold rotation axis in the *a* direction. The possible diffraction groups for a 2*mm* whole pattern symmetry are 2*mm* and 2*mm*1*R*. Diffraction group 2*mm* has possible point groups of *mm*2 and $\bar{6}m2$ while 2*mm*1*R* has possible point groups of *mmm*, 4/*mmm*, 6/*mmm*, *m*3, and *m*3*m*. The choices of the point group are narrowed down to 4/*mmm*, as this is

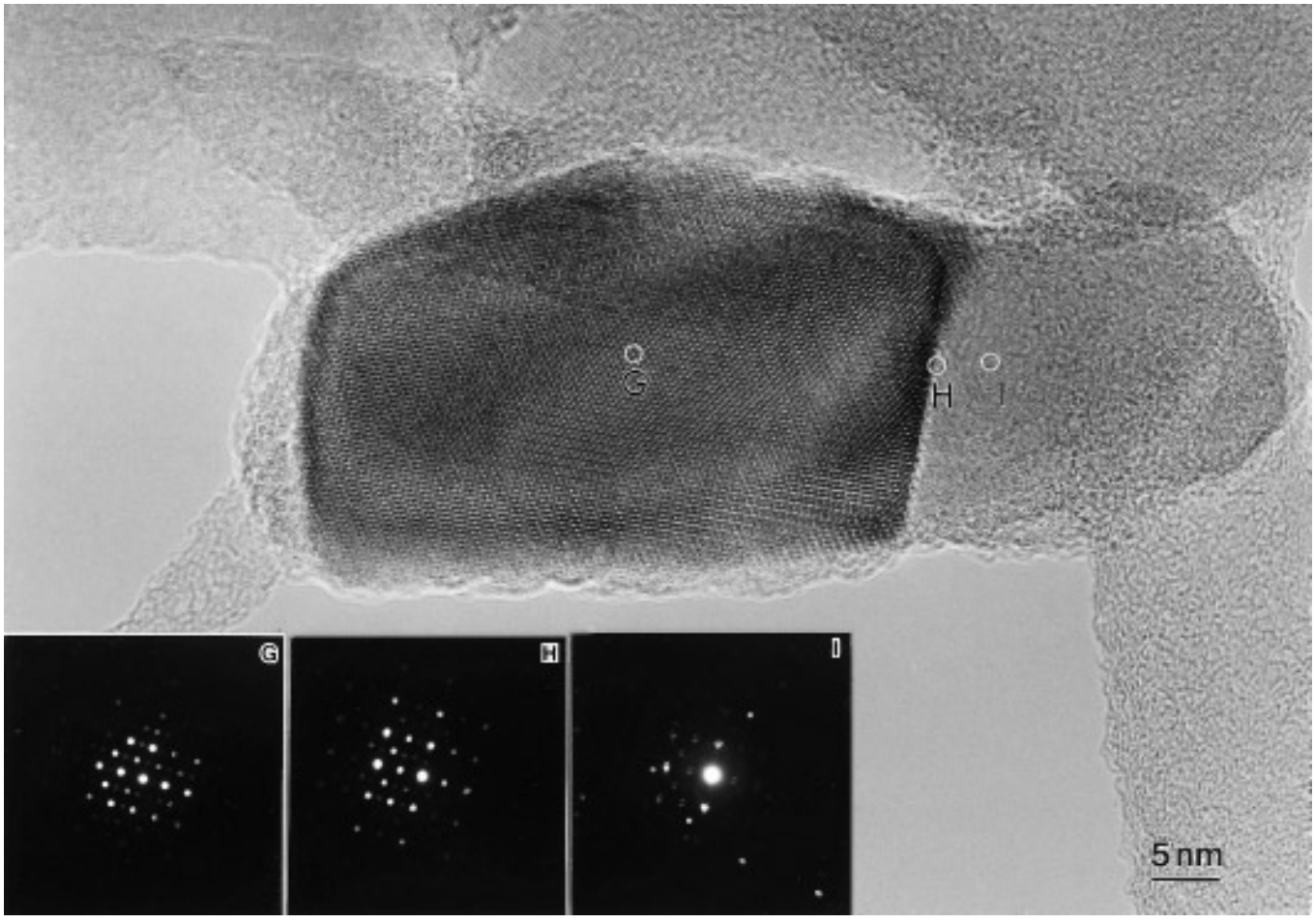

FIG. 7. High resolution image showing a $CaFeTi_2O_6$ crystal consists of two different domains; one is highly ordered and the other is highly disordered. Insert shows the electron diffraction patterns collected using a 1 nm electron probe from regions marked as G, H, and I, showing that the same crystal orientation remains in all three regions.

the only group consistent with both orientations. Therefore, the point group is uniquely determined as $4/mmm$.

3.3. Unit Cell Determination

The next step toward space group determination is to identify the unit cell type. This can be done by examining experimentally obtained absences and extinction rules. The rule of forbidden reflection along [001], [100], [110], and [331] (Figs. 3a–d) is found to be $hk0$: $h + k = 2n$, and hhl: $l = 2n$. Further analysis showing that in addition to providing information on the crystal symmetry elements, the positions of the FOLZ reflections can also be utilized to identify possible crystal structures. As shown in Fig. 1, upon superimposing the FOLZ reflections on the ZOLZ reflections along both [010] or [100] direction, it is found that the resultant displacement vector is equal to zero. This confirms that the real space unit cell of $CaFeTi_2O_6$ is primitive (P).

3.4. Space Group Determination

The last and the most critical step in the determination of the space group consists of determining which of the mirrors and rotation axes that occur in the point group are in fact glide planes or screw axes. According to the selected-area electron diffraction patterns shown in Fig. 3, the following extinction rule is established: for [001] zone, $hk0$: $h + k = 2n$; for [110] zone, hhl: $l = 2n$, $00l$: $l = 2n$. However, the extinction rule along a [100] zone can not be established due to the complexity caused by the dynamic electron scattering. As shown in Fig. 3b, there is no restriction to l for the $00l$ reflection. The appearance of $0k0$ and $00l$ (k, l: odd) reflections makes it very difficult to identify a screw axis 4_2 along c in this case. Therefore, we use a more sophisticated method (G–M line analysis) to complete this investigation.

Glide planes and screw axes produce clearly identifiable features in CBED patterns and these features are used to

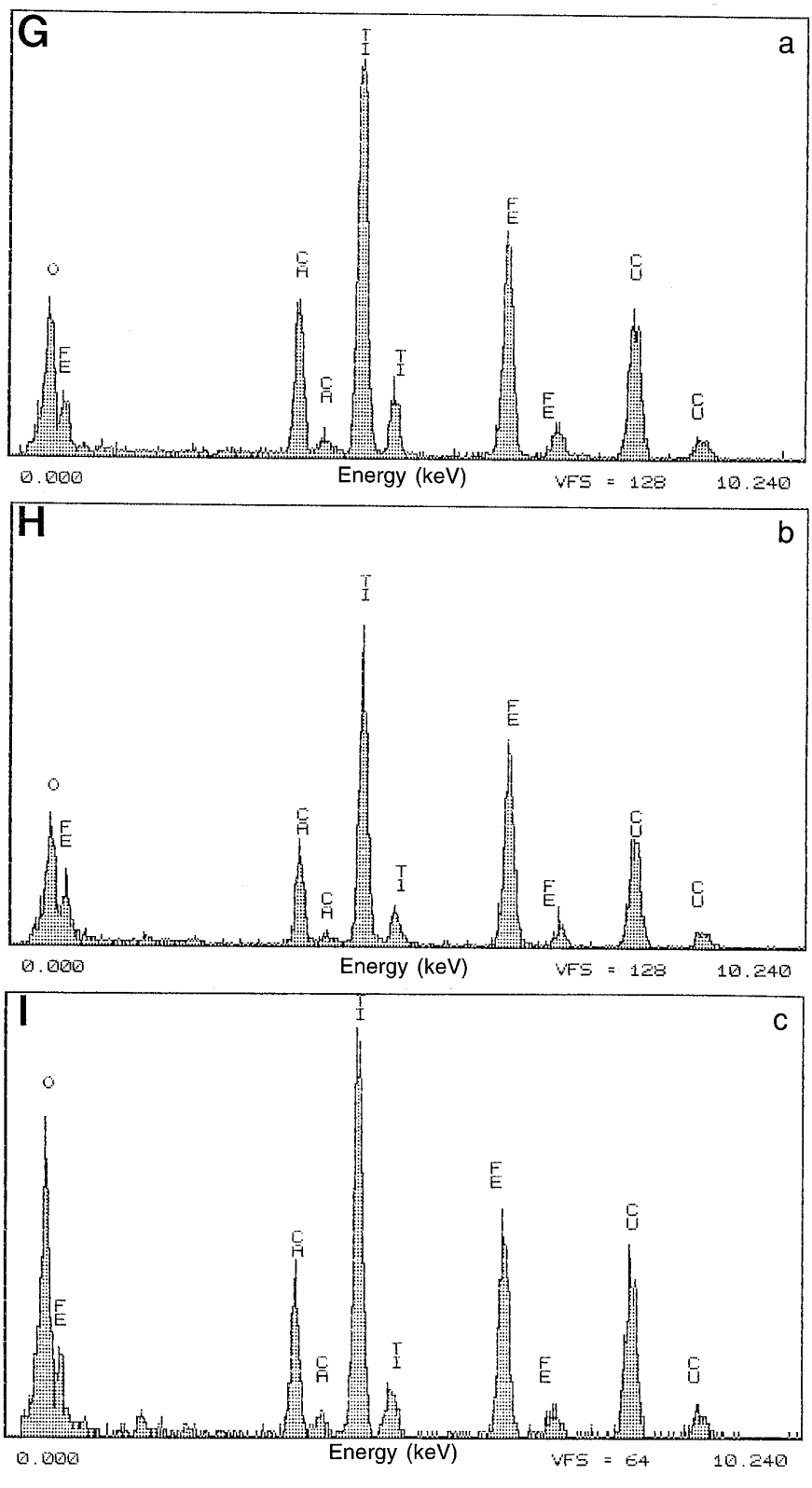

FIG. 8. EDX spectra collected from various regions shown in Fig. 7 using a 1 nm electron probe, with (a) region G, (b) region H, and (c) region I, respectively.

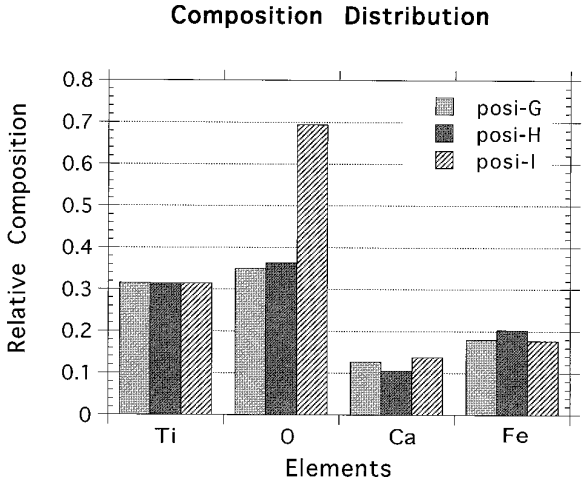

FIG. 9. Summary of elemental compositions for EDX spectra shown in Fig. 8. Note that the oxygen content is about a factor of two higher in region I than the other two regions.

deduce the presence of the symmetry elements (4, 7–11). These identifiable features are normally zeros in the diffraction intensity, known as dynamical extinctions or Gjonnes and Moodie (G–M) lines. Dynamical extinctions occur only in reflections that are kinematically forbidden as a result of the presence in the crystal structure of glide planes and/or twofold screw axes (2_1). G–M lines are the ''fingerprinting'' of the crystal phase and the usage of them normally lead to an unambiguous assignment of the space group (10–13). According to the International Tables for X-ray Crystallography (14) or The Dynamic Extinction Tables of Space Groups (8), there are 16 possibilities (space groups No. 123 to No. 138) among the 230 space groups which have the point group 4/*mmm* with lattice type (P). Detailed insepction of Fig. 2b, which is a [100] zone axis ZOLZ-CBED pattern, reveals that dynamic extinctions (G–M lines) are exactly excited in every alternate reflection ($0k0$) (k: odd). The presence of G–M lines of A_2 type (seen as a radial dark line) indicates that there is a *b*- or *n*-glide plane perpendicular to the *c* axis and/or a 2_1 screw

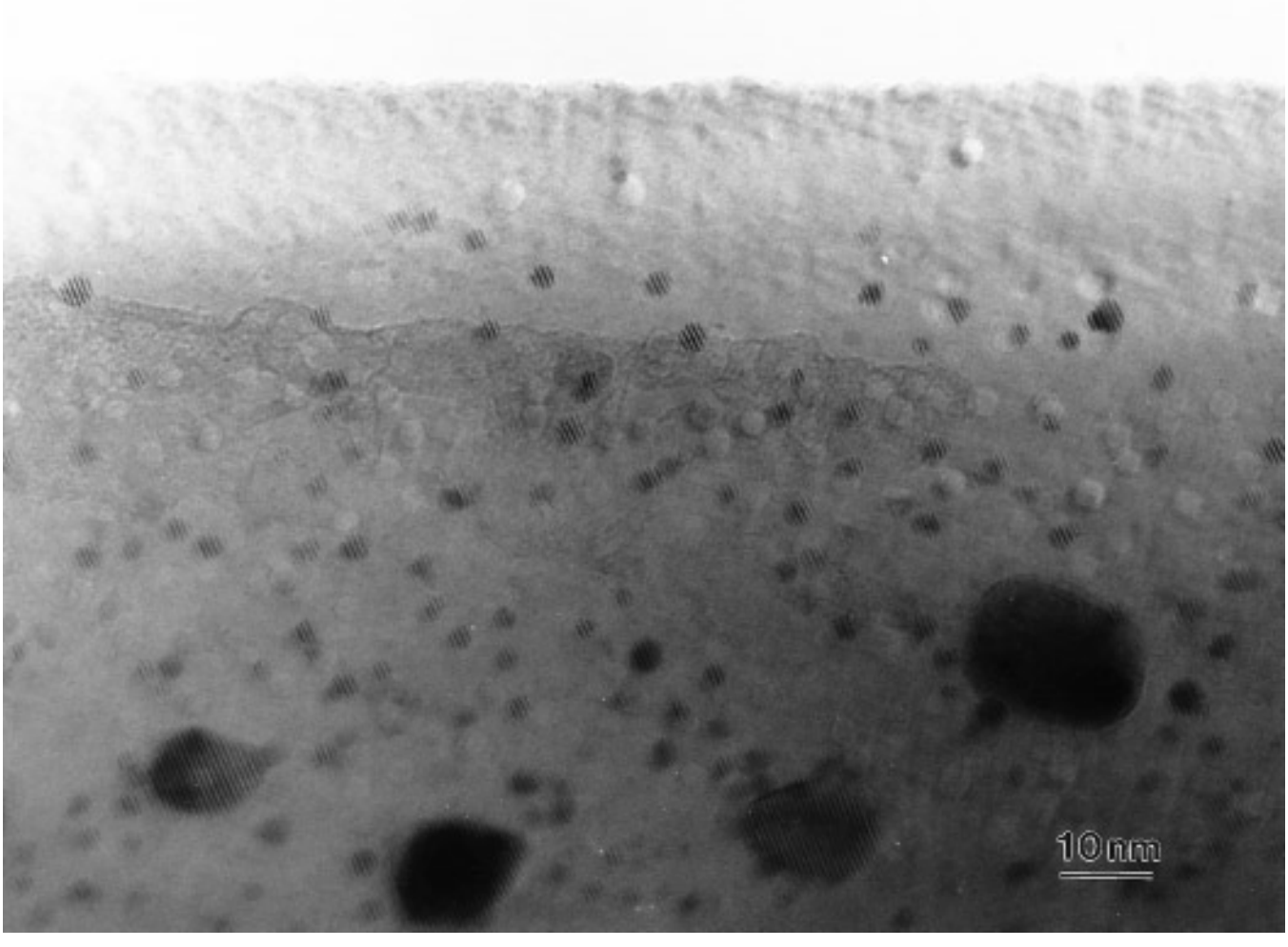

FIG. 10. High resolution image showing that $CaFeTi_2O_6$ contains two sizes of iron precipitates. One size class averages 4 nm in diameter and the other size class averages 15 nm in diameter (bar = 10 nm).

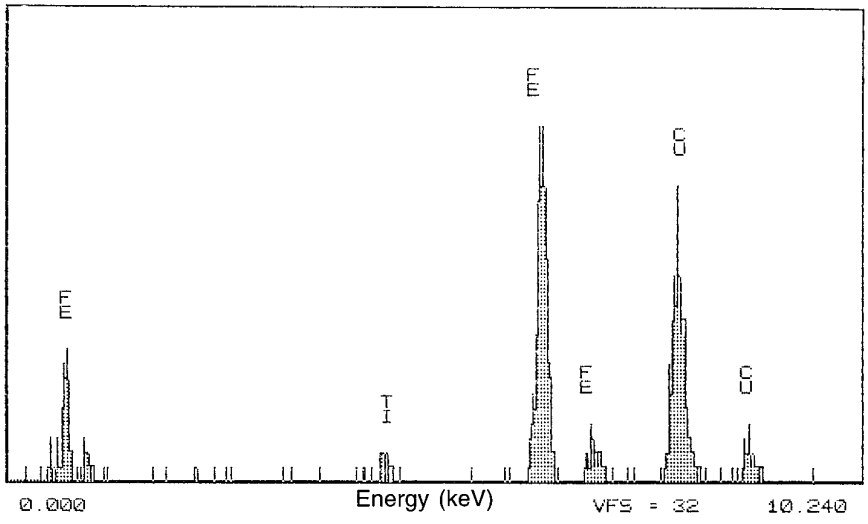

FIG. 11. EDX spectrum from one of the dark precipitates in $CaFeTi_2O_6$ matrix in Fig. 10, showing the dominant Fe peaks.

axis parallel to the *b* axis. Among 16 possible space groups only space groups $P4/nmm$ (No. 129), $P4/ncc$ (No. 130), $P4_2/nmc$ (No. 137), and $P4_2/ncm$ (No. 138) meet these requirements (Table 1) (8). To further deduce symmetry elements, we need to obtain other zone axis CBED patterns and examine them for the presence of dynamic extinctions (G–M lines). Figure 4 is a CBED pattern along the $[h0l]$ (h: 1, l: 1) zone axis. The dynamic extinctions (G–M lines) of the A_2 type appear in the ZOLZ (010) and (0-10) reflection discs, but not the (-101), (10-1) reflection discs. Based on this analysis, the space group of the crystal is deduced to be either $P4/nmm$ (No. 129) or $P4_2/nmc$ (No. 137). Last, the CBED pattern at the $[hhl]$ (h: 1, l: 2) zone axis is examined (Fig. 5). Both dynamic extinctions (G–M lines) of A_2 and B_2 types are seen in alternate reflections ($\bar{1}\bar{1}1, 11\bar{1}, 33\bar{3}$, etc.). It is clear that only the space group $P4_2/nmc$ satisfies these experimentally observed criteria. Therefore, the correct space group of $CaFeTi_2O_6$ is uniquely determined to be $P4_2/nmc$ (No. 137), confirming the space group assignment proposed by X-ray diffraction (1).

3.5. Low Temperature Crystal Structure and Symmetry

CBED patterns at ambient temperature were examined for $CaFeTi_2O_6$ crystal oriented along several high symmetry directions, such as [001] and [100]. After cooling to 84 K these same orientations were again examined. It was possible in all cases to follow the CBED from the same region of a crystal aligned near a chosen orientation through the *in situ* cooling experiment. At ambient temperature, limited information is available from CBED pattern due to weak and thermally diffuse scattering. Beam sensitivity (radiation damage) also limits the information that can be extracted. Despite these limitations, the information is still sufficient to compare with low temperature patterns. CBED patterns at 84 K are found to have identical whole pattern symmetry and to be consistent with a tetragonal lattice having $a = 7.51 \pm 0.02$ Å, $c = 7.54 \pm 0.02$ Å. Local structure also has been examined by displacing the electron probe across the small crystallite. There are no extra spots or variations in the diffraction pattern, suggesting that the crystal ordering is quite stable over the low temperature range from 300 to 84 K.

3.6. High Resolution Imaging and Nanobeam Analysis

The possibility of defects, ranging from dislocations and twinning to variations in degree of order and stoichiometry, exists in materials synthesized at high pressure and temperature. High resolution lattice imaging is a powerful tool to examine such imperfections. The local atomic structure of the $CaFeTi_2O_6$ crystal was investigated by HREM; Fig. 6 shows an example. This image was taken at near Scherzer defocus with electron beam incidence along the [001] direction at 200 KeV from a very thin crystal (<50 Å). The nearly perfect lattice image shows considerable structural homogeneity. Careful examination of numerous crystals with different orientations using both HREM and SAED shows no gross defects such as dislocations or massive faults. The majority of $CaFeTi_2O_6$ crystals (~75% of examined crystallites) have such nearly perfect structure. This indicates that $CaFeTi_2O_6$ perovskite is generally structurally homogeneous.

The measurement of local lattice parameter with variations in the local composition enable us to further investigate the properties of this new compound. Figure 7 is a high resolution image of a crystal with domains of two different crystallinities. Such crystals are relatively rare. The region on the left (region G) shows a regular lattice

image while the region on the right (region I) presents a quasi-crystalline or amorphous-like morphology. These two regions are divided by a boundary (region H). There is a sudden loss of long-range order in region I, compared to region G. The insert in Fig. 7 is the corresponding nanodiffraction patterns taken from the above regions with a 1 nm incident electron beam along a direction close to the [110] zone axis. Detailed inspection of these diffraction patterns marked as G, H, and I reveals that although different diffraction characteristics appear in the image, all domains retain the same crystal orientation (with [110] surface normal almost parallel to the incident beam direction) and there are no variations in lattice parameters when crossing the interface. This indicates that short-range (subnanometer regime) ordering exists in region I. The composition in these regions was determined by EDX analysis with the same probe size as shown in Figs. 8a–8c. The analysis of these spectra is summarized in Fig. 9. The oxygen concentration in region I is about a factor of two higher than that in the other two regions, suggesting that oxidation might be directly responsible for the high degree of disordering observed. The formation of this type of domain may be attributed to local variations of stoichiometry with considerable oxidation. The distribution of this nonstoichiometric phase might affect chemical and physical properties. Further study could correlate the distribution of this phase with a possible reaction sequence during synthesis, or with structural principles relating possible new phases and, hence, suggest reaction mechanisms.

High resolution imaging and nanobeam analysis also reveal that in addition to the major $CaFeTi_2O_6$ oxide phase and the oxidized minor phase, there is a third phase in the material synthesized from an equimolar mixture of $CaTiO_3$ and $FeTiO_3$. Figure 10 is a high resolution image taken from a crystal region of different morphology along the [001] orientation. This image shows that there are two sizes of precipitates. One size class averages 4 nm in diameter and the other 15 nm in diameter. Nanobeam diffraction and analysis indicate those precipitates are iron particles in the $CaFeTi_2O_6$ matrix. The lattice fringes in the matrix belong to the {110} $CaFeTi_2O_6$ crystal planes. The relatively large fringe spacing (known as Moire fringes) is due to the small misfit between parallel reflection from Fe precipitates and $CaFeTi_2O_6$ matrix. The spacing D_M of the Moire fringes is given by $D_M = d_1d_2/|d_1 - d_2|$ (15), where d_1 and d_2 are the d-spacings of two overlapping sets of crystal planes, one of Fe and the other of $CaFeTi_2O_6$. To satisfy the lattice image and the analysis of Moire fringes, the orientation relationship between $CaFeTi_2O_6$ and Fe precipitate can be derived as $\{110\}_{CaFeTi2O6}//\{100\}_{Fe}$. Based on the observation that the structure is well described by the equilibrium crystal structure of bulk Fe, we conclude that the precipitates consist of almost pure Fe. This is further confirmed by nanobeam EDX analysis collected from an individual precipitate as shown in Fig. 11. Fe atoms probably cluster together by solid phase transformation, presumably through a nucleation and growth mechanism. These Fe crystallites of relatively large size (up to 15 nm) maintain a well defined orientation relationship with the $CaFeTi_2O_6$ crystal matrix. The observation of Moire fringes parallel to {110} set of planes indicates that {110} planes serve as an interface for the epitaxial crystallization of Fe precipitates at some stage of synthesis. The coexistence of oxidized regions and iron precipitates in the same sample is noteworthy. It may result from several factors; (i) the $FeTiO_3$ starting material (made from Fe, Fe_2O_3, and TiO_2 by a sealed-tube technique) may contain small regions of not fully reacted material; (ii) the high pressure synthesis may respond to gradients in oxygen fugacity, hydrogen fugacity, or temperature; (iii) a more oxidized perovskite, perhaps in the brownmillerite series $CaFeO_{2.5}$–$CaTiO_3$ (16), may be the intermediate during synthesis. Further study is needed.

ACKNOWLEDGMENTS

The authors acknowledge Mr. M. Kawasaki and Mr. K. Ibe of JEOL, Ltd. for assistance in obtaining the nanobeam analytical result. This work was made use of MRSEC Shared Facilities supported by the National Science Foundation under Award DMR-940032. This research was supported by the Center for High Pressure Research, an NSF Science and Technology Center.

REFERENCES

1. K. Leinenweber, and J. Parise, *J. Solid State Chem.* **114,** 277 (1995).
2. K. Leinenweber, J. Linton, A. Navrotsky, Y. W. Fei, and J. Parise, *Phys. Chem. Miner.*, in press.
3. J. M. Cowley, ''Diffraction Physics.'' North-Holland, Amsterdam, 1975.
4. B. F. Buxton, J. A. Eades, J. W. Steeds, and G. M. Rackham, *Phil. Trans.* **281,** 171 (1976).
5. K. K. Fung, S. McKernan, J. W. Steeds, and J. A. Wilson, *J. Phys. C. Solid State Phys.* **14,** 5417 (1981).
6. N. Yao, C. F. Klein, S. K. Behal, M. M. Disko, R. D. Sherwood, D. M. Cox, *Phys. Rev. B* **45,** 19, 11366 (1992).
7. J. Gjonnes and A. F. Moodie, *Acta Crystallogr.* **19,** 65 (1965).
8. M. Tanaka, H. Sekii, and Nagasawa, *Acta Crystallogr. A* **39,** 825 (1983).
9. M. Raghavan, J. Y. Koo, and R. Petkovic-Luton, *J. Metals* **35,** 44 (1983).
10. M. Tanaka, H. Sekii, and T. Nagasawa, *Acta Crystallogr. A* **50,** 261 (1994).
11. J. A. Eades, *in* ''Electron Diffraction Techniques'' (J. M. Cowley, Ed.), Vol. 1, p. 313. Oxford Science Publications.
12. J. F. Mansfield, R. J. Graham, and Y. P. Lin, *Norelco Report* **33** (1EM), 54 (1986).
13. D. J. Eaglesham, *J. Electron Micro. Tech.* **13,** 66 (1989).
14. ''International Tables for Crystallography'' (T. Hahn, Ed.), Vol. A. Space-Group Symmetry, International Union of Crystallography, 1983.
15. J. W. Edington, ''Practical Electron Microscopy in Materials Science.'' p. 190. Van Nostrand Reinhold Company, NY, 1976.
16. T. R. S. Prasanna, and A. Navrotsky, *J. Mater. Res.* **9**(12), 3121 (1994).